Understanding the origin of liquid crystal ordering of ultrashort double-stranded DNA

Suman Saurabh, Yves Lansac, Yun Hee Jang, Matthew A. Glaser, Noel A. Clark, and Prabal K. Maiti

Understanding the Origin of Liquid Crystal Ordering of Ultra-Short Double Stranded DNA

Suman Saurabh[1,2], Yves Lansac[2,3], Yun Hee Jang[4], Matthew A. Glaser[5], Noel A. Clark[5], and Prabal K. Maiti[1]

[1]*Center for Condensed Matter Theory, Indian Institute of Science, Bangalore, India.*
[2]*GREMAN, Université François Rabelais, CNRS UMR 7347, 37200 Tours, France.*
[3]*Laboratoire de Physique des Solides, CNRS, Université Paris-Sud,*
Université Paris Saclay, 91405 Orsay cedex, France.
[4]*Department of Energy Systems Engineering, DGIST, Daegu 42988, Korea. and*
[5]*Department of Physics and Liquid Crystal Materials Research Center,*
University of Colorado, Boulder, CO 80309, USA.
(Dated: February 13, 2017)

Recent experiments have shown that short double-stranded DNA (dsDNA) fragments having 6- to 20- base pairs exhibit various liquid crystalline phases. This violates the condition of minimum molecular shape anisotropy that analytical theories demand for liquid crystalline ordering. It has been hypothesized that the liquid crystalline ordering is the result of end-to-end stacking of dsDNA to form long supra-molecular columns which satisfy the shape anisotropy criterion necessary for ordering. To probe the thermodynamic feasibility of this process, we perform molecular dynamics simulations on ultra-short (4 base pair long) dsDNA fragments, quantify the strong end-to-end attraction between them, and demonstrate that the nematic ordering of the self-assembled stacked columns is retained for a large range of temperature and salt concentration.

Sequence-directed self assembly (SDSA) is the defining operational characteristic of DNA polymers, developed by living matter to store and transmit information , and currently being used in DNA nanotechnology to design and program nanostructure formation and motion [1, 2]. A particularly interesting but relatively less explored mode of DNA SDSA is found in ultra-short DNA oligomers [3]: in mixed aqueous solutions of complementary and non-complementary ultra-short DNA strands, those that are complementary pair up to make short duplexes. If the attractive interactions between their terminal base pairs is strong enough, these duplexes can, in turn, aggregate end-to-end to form molecular stacks, which can then order into a columnar liquid crystal phase. The resulting chromonic LC ordering [4] appears at sufficiently high DNA concentration via a first order phase transition in the form of condensed LC droplets of complementary oligomers surrounded by isotropic solution of non-complementary oligomers [5]. That is, the SDSA-enabled liquid crystal order acts as a molecular selector, physically collecting sufficiently complementary and attractive oligomers. In the presence of appropriate abiotic ligation chemistry, the physical proximity and organization of reacting duplex end-groups, characteristic of the LC ordering, strongly accelerates ligation of duplex oligomers into longer polymers in the LC phase [6, 7]. Since the LC ordering in turn becomes more stable as oligomer length increases, this ligation is effectively auto-catalytic, a step in a positive feedback loop, known as liquid crystal auto-catalysis (LCA) [6], that promotes LC ordering and oligomer lengthening.

LC ordering of duplex DNA has been reported for complementary oligomers as short as 6 bases, and LC auto-catalysis has currently been demonstrated for oligomers as short as 12 bases [6, 7]. An exciting challenge is to extend these observations to shorter oligomers and ulti-

mately solutions of single bases, which then could be considered as models for the process that led to the appearance of sequence-directed self assembling polymers in the pre-biotic era [8]. Phase behaviour of a collection of rod-shaped molecules has been extensively investigated both theoretically and experimentally [9-32]. However, understanding how the key steps of duplex aggregation and LC formation depend on oligomer length and sequence is both virtually unexplored and strongly dependent on the molecular details of oligomer interaction. These conditions motivate in this paper the use of atomistic molecular dynamics simulations to explore duplex aggregation and LC formation in oligomeric systems of 4-bp dsDNA.

We consider both blunt-end (GTAC) and shifted-end (GCTA) DNA fragments with a two-base overhang on each strand (Figure S2) [33]. To demonstrate that the end-to-end stacking is energetically favourable up to very small DNA length scales, we calculate the potential of mean force (PMF) between the DNA fragments and find strong attractive interaction for both blunt-end and shifted-end DNAs. We perform MD simulations on pre-formed columns made of 4-bp DNA fragments initially assembled in a hexagonal arrangement at different DNA volume fractions, temperatures and salt concentrations. We observe nematic ordering for high volume fractions which gradually changes to a weakly ordered phase as the DNA volume fraction is lowered.

I. METHODS

DNA model build-up .– NAB (Nucleic Acid Builder) module of AmberTools12 was used to prepare all the systems which were solvated with the SPC/E water model [34] and neutralized by adding a proper number of Na$^+$ ions using the xleap module of AMBER12 [35]. The ff10

force field which includes the parmbsc0 correction [36] was used to describe the DNA fragments. The ions are descrbed using the Joung-Cheatham parameter set [37].

MD protocol .– The systems were minimized for 1000 steps using the steepest descent minimization method and followed by 2000 steps of conjugate gradient minimization. During the minimization all the atoms in the DNA fragments were held fixed in their starting conformation using harmonic constraints with a force constant of 500 kcal/mol/Å^2. This allowed water molecules to reorganize and eliminate unfavorable contacts with DNA. After this, 5000 steps of conjugate gradient minimization were performed, decreasing the force constant (in kcal/mol/Å^2) from 20 to 0 by a step of 5 every 1000 steps. After minimization, these systems were heated from 0 K to 300 K (in some cases 280 K) within 40 ps, while the solutes were held fixed using harmonic constraints with a force constant of 20 kcal/mol/Å^2. The SHAKE constraints [38] were applied on all the bonds involving hydrogen atoms with a tolerance of 5×10^{-4} Å. The temperature regulation was achieved using the Berendsen weak coupling method [39] with a temperature coupling constant of 0.5 ps. All the simulations are performed using the PMEMD module [40] of AMBER12. The particle mesh Ewald (PME) method with a real space cut-off of 9 Å is used to estimate the long-range electrostatic interactions. The visualization of the MD trajectories was done using VMD [41].

PMF calculation .– The PMF calculations between a pair of DNA fragments restrained in specic congurations are performed using the umbrella sampling (US) method [42], which allows for an efficient sampling of the phase space by performing a set of simulations (windows) along a reaction coordinate (RC) under an additional harmonic biasing potential. At each window, the system is rst minimized using the protocol described above and then equilibrated by MD simulations at constant pressure and constant temperature (NPT) for the duration of 2 ns. The pressure regulation is achieved using the Berendsen barostat [39] with a pressure relaxation time of 0.5 ps. Then nally a 10 to 12 ns of NVT MD simulation is performed at each window and the trajectory collected after discarding the first 2 ns is used to construct the PMF using the weighted histogram analysis method (WHAM) [43]. The details of the restraints employed is provided in section S1 [33].

Assembled DNA columns .– We use the NAB module to build stacked columns of blunt-end and shifted-end DNA fragments. Each column consists of five 4-bp DNA fragments. The blunt-end DNA columns are of two types, one with consecutive DNA fragments in the following helix conformation and the other with consecutive fragments in the same-helix conformation (see Figure S5) [33]. Another type of DNA columns, consisting of shifted-end fragments, is also prepared. A total of 18 columns are placed in a hexagonal arrangement. By varying the thickness of the water layer around the 18-column system as 10 Å, 15 Å, 25 Å and 30 Å, we pre-

pare four systems with different DNA volume fractions (Φ) of 52 % (54 %), 40 % (44 %), 31 % (34 %), and 20 % (21 %), respectively, for the blunt-end (shifted-end) DNA systems. The system size varied from 105 atoms for the highest volume fraction to 3×10^5 atoms for the least. A total of 540 Na^+ ions are added to neutralize the charge on the DNAs. The systems are minimized and heated to a temperature of 280 K followed by NPT simulations longer than 150 ns. We also performed simulation of blunt-DNA columns at 150mM and 75mM NaCl at Φ = 52 % . 94 Na^+ and Cl^- ions were added to attain a salt concentration of 150mM, while 47 ions were added to generate the system with 75mM salt.

II. RESULTS AND DISCUSSION

Blunt-end DNA: End-to-end PMF.– To evaluate the effective interaction responsible for the formation of a multi-fragment column of DNA, we first calculate the PMF between a pair of blunt-end DNA fragments (figure S2A) [33], which are stacked on top of each other such that they have a common long axis (Figure 1A). The distance between the two centers of mass (COM) of the nearest base-pairs (end-to-end distance) is defined as the reaction coordinate (RC) (Figure 1A) and the long axes of the fragments are forced to align in the same direction in the simulations. The PMF is calculated at 300 K for two different DNA configurations. One with the two DNA fragments stacked in a way that the twist between their nearest base pairs was similar to a continuous B-form DNA (following-helix (FH)) (Figure 1A) and another with one DNA just translated with respect to other along their common long axis (same-helix (SH)) (Figure 1B).

The PMF profile for the FH configuration shows an attractive interaction of 10 kcal/mol at an end-to-end distance of 3.75 Å (Figure 1A), where the bases at the interface are well shielded from water in a closed configuration. The PMF calculation repeated for the SH configuration, where the interfacial bases are exposed to water in an open configuration, shows an attractive interaction of 6 kcal/mol with a minimum at an end-to-end distance of around 4 Å (Figure 1B). The difference in stabilization for the two configurations illustrates the hydrophobic origin of the end-to-end short-range attraction. In a simulation of two axially aligned DNA fragments kept a small distance apart, we observe a very swift approach and stacking in the FH configuration at a distance of 3.75 Å validating the above observations (Figure S3A-B) [33]. Our binding energy values are consistent with the value (6.3 kcal/mol) obtained by Aksimentiev et al [44] for the end-to-end stacking of 10-bp long dsDNA which were free to rotate about their common axis contrary to ours. Being free to rotate, the azimuthal sampling of their DNA fragments and hence the accessibility of the interfacial bases to water due to thermal uctuations is in-between the two congurations that we have

used, resulting in an intermediate value of binding energy. Although their value of 6.3 kcal/mol seems close to the value of 6 kcal/mol that we obtain for the SH configuration, one must note that a longer DNA sequence would lead to a larger positive electrostatic contribution resulting in raising of the PMF minimum.

It is important to point out that the stacking free energies obtained by us are larger than the values (1-2 kcal/mol) predicted by the Santa Lucia model [45] for a DNA quadruplet. Also, the experimental values for DNA-DNA stacking free energy range from 2-4 kcal/mol [46]. In experiments, the azimuthal freedom of the DNA molecules forming the stack leads to a stacking conformation with a stacking area larger than that found in base-pair stacks within a DNA helix [47]. Whereas, we find that even in the SH configuration, which corresponds to low stacking area, we obtain a value of 6 kcal/mol for the free energy of binding. The higher values seem to stem from the nature of the force fields, which have a tendency of overestimating the stacking free energies [48, 49]. This overestimation will lead to columns that are rigid and would stabilize the nematic phase at higher temperatures.

Shifted-end DNA.– In the case of a pair of shifted-end DNA fragments (Figure S2B) [33], the COM of the two bases constituting the overhang is defined for each DNA fragment and the distance between the two COMs is taken as RC for the PMF calculation (Figure 1C). We again find a comparable stabilization energy of 9 kcal/mol (Figure 1C) at a minimum-energy distance of 10.6 Å. Indeed, in a simulation where a pair of shifted-end DNA fragments are placed at an initial distance of 17.5 Å and left to evolve without any restraints, the two DNA fragments approach each other and settle at a distance of around 10.6 Å within 0.6 ns (Figure S3C of). A discussion on the temperature dependence of the PMF between two shifted-end DNA fragments is presented in section S4 [33].

Blunt-end DNA: Side-by-side PMF.– Now that inter-DNA interaction is shown to be strong enough to form a multi-fragment column, we calculate the PMF between a pair of blunt-end DNA fragments placed side-by-side (Figure 1D).The side-by-side interaction between DNA fragments has been studied in some detail previously [50–52]. Seidel et al. [50] demonstrated that in the presence of monovalent ions, the effective repulsion between DNA supercoils corresponds to 40 % of the DNA charge. Thus, it is important to examine whether ultra-short DNA fragments show electrostatic repulsion sufficient to give rise to considerably anisotropic interaction that would lead to the formation of columns. The COM of each DNA fragment is defined using the two non-terminal bases and the distance between the COMs is chosen as RC (Figure 1D), while the long axes of the two DNA fragments are kept parallel to each other. The DNA fragments are initially placed such that they have the same orientation with respect to their long axes(Figure S5) [33], and are free to rotate about their long axes. Similar simulations starting
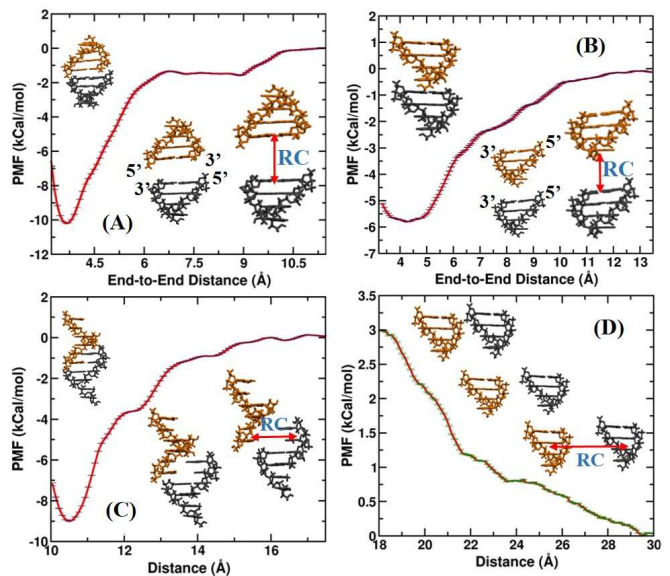
FIG. 1. PMF profiles at 300 K for a pair of 4-bp DNA fragments. End-to-end PMF for blunt-end DNA (GTAC) fragments in (A) FH configuration and (B) SH configuration. (C) PMF for shifted-end DNA (GCTA) as well as (D) PMF for blunt-end DNA fragments placed side-by-side. The insets show the definition of the reaction coordinates for each PMF calculation and the initial systems corresponding to different windows along the reaction coordinate.

from different initial relative orientations (90°, -90° and 180°) are also performed and shown in section S5 [33].

The PMF profile (Figure 1D) shows only repulsive interaction, decreasing monotonically with increasing separation. The repulsive barrier to bring them to short distances (∼19 Å) is as high as 3 kcal/mol (∼5 k_BT) and is attributed to the electrostatic repulsion between like-charged DNA fragments, since PMF calculations performed with the DNA fragments free to topple (section S5) [33] show significantly reduced (down to 1-2 k_BT) electrostatic repulsion at short separations through near-perpendicular relative orientations of the DNA long axes. DNA fragments, initially placed side by side and restrained at a very small COM-to-COM distance (∼19 Å) but not restrained to stay in the side-by orientation, finally attain a stacked conformation (Figure S5) [33].

It is clear that the DNA-DNA interaction is anisotropic: the fragments repel each other sideways but attract strongly end-to-end. This anisotropy as well as the strength of the interactions lead to the formation of stable blunt-end and shifted-end DNA columns.

Liquid Crystal phase of short dsDNA.– The inter-DNA interaction leads to columns which could subsequently order to form LC phases at high enough concentration (Figure 2A). The behavior of the LC phase is examined using MD simulations on a collection of multiple dsDNA columns (Figure 2) placed on a hexagonal lattice at different values of Φ. We performed such simulations on three different systems (Figure S6) [33]. The first system

had blunt-end DNA fragments forming columns with an initial SH configuration between consecutive fragments. The second system consisted of blunt-end DNA fragments initially in a FH configuration. The third system had columns consisting of shifted-end DNA fragments. At their respective highest volume fractions (52 % for blunt-end system and 54 % for shifted-end system), the systems relax to a nematic LC phase. The snapshots of one of the systems at the highest and lowest volume fractions are shown in Figure 2B-C. We calculate the nematic order parameter (S_2) by first evaluating the second-order tensor $S_{\alpha\gamma}$ given by $(1/N) \sum_{i=1}^{N} [\nu_\alpha^i \nu_\gamma^i - \frac{1}{3}\delta_{\alpha\gamma}]$, where ν_α^i is the α cartesian component of the vector that defines the long axis of the DNA molecule i (defined as the line joining the centers of mass of the terminal base pairs of the molecule) and δ is the kronecker symbol. The tensor is then diagonalized and the largest eigenvalue is used as the order parameter S_2 for the system. Figures S7A-C [33] show the time evolution of the nematic order parameter for the three systems at each volume fraction at a temperature of 280 K. At their respective highest volume fractions, the systems relax to a nematic LC phase. For example, S_2 saturates at around 0.7 after 200 ns long simulations for the blunt-end DNA systems at Φ of 52 %. For Φ of 20 %, S_2 attains a small value of around 0.2 which is a signature of an isotropic phase (or at least a weakly ordered nematic phase). It is worth mentioning that the largest eigenvalue of the order parameter tensor scales as $N^{-1/2}$, where N is the total number of anisotropic molecules [53]. So, with only 18 DNA columns, we obtain considerably large values for S_2 even in the isotropic phase. The average order parameter for the last 50 ns of each simulation, as a function of Φ, is shown in Figure 3A. It is worth mentioning that DNA, being a chiral molecule, also exhibits chiral-nematic phase, but the cholesteric pitch length is of the order of micrometer [54]. So, in an atomistic simulation, it is not possible to observe this phase, as the pitch length is several orders of magnitude larger than the individual dsDNA length, and it would require a very large system to accommodate the cholesteric pitch. In addition, the atomistic approach prohibits a director description of the system, as the directional fluctuation of the directors occurs over a length scale much larger than the system size.

To see the effect of temperature, we simulated the SH blunt-end DNA system at high volume fraction ($\Phi = 52$ %) and at higher temperatures of 300 K and 343 K. Nematic ordering is still very high at 300 K and remains very significant even at 343 K (Figure 3B). The large temperature range of existence of the nematic phase, as discussed before, is due to the strong inter-DNA stacking interaction.

The effect of salt concentration on the nematic order was explored by performing simulation of FH blunt-end dsDNA columns at 150 mM and 75 mM NaCl at Φ of 52 %. Although nematic ordering is still very high, we find that average S_2 of the systems in presence of salt is slightly lower as compared to the no-salt system (Fig-
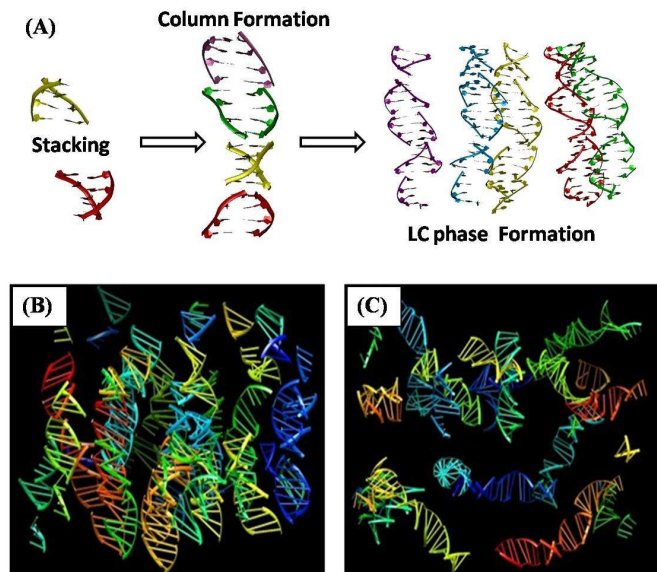
FIG. 2. (A) Mechanism of LC phase formation in aggregates of ultra-short dsDNA. (B) Nematic phase of blunt-end (GTAC) DNA system with SH initial configuration for Φ of 52 % at 280 K (C) Isotropic phase of blunt-end DNA system with SH initial configuration for Φ of 20 % at 280 K.
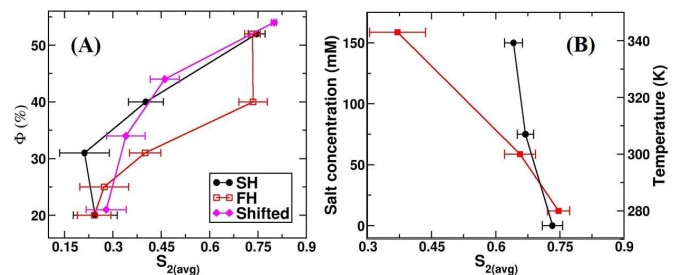
FIG. 3. (A) Average nematic order parameter at different volume fractions (Φ) for different systems at 280 K. (B) Variation of order parameter with salt concentration (black) for blunt-end DNA (GTAC) system with an initial FH configuration at Φ of 52 % and temperature (red) for blunt-end DNA (GTAC) system with an initial SH configuration at Φ of 52 %.

ures S7D [33] and 3B). This effect may arise due to a reduction in the side-by-side electrostatic repulsion between the DNA columns (due to charge screening) leading to a relatively weakly packed system. The result is in agreement with earlier works studying the LC phases of polyelectrolytes and DNA aggregation [55], which predict that as the charge of the monomer units constituting the charged rods increases, the system shows a transition to the isotropic phase at lower and lower number of monomers constituting the rod. While, as the salt concentration goes up, the transition line shifts towards higher number of monomer units. So, with larger electrostatic screening, aggregates of longer rods show a disordered arrangement. This behavior has also been pre-
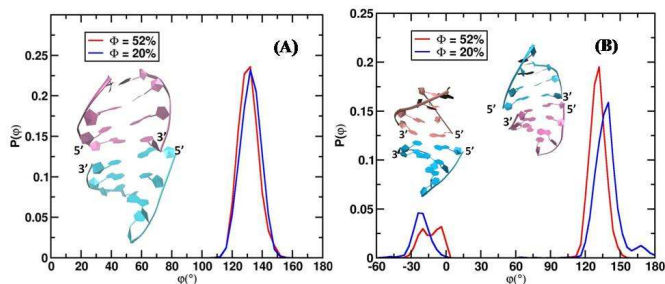
FIG. 4. (A) φ distribution for blunt-end DNA (GTAC) system with FH initial configuration and (B) SH initial configuration for Φ of 52 % and 20 % at T = 280K.

dicted theoretically by De Michele et al. [56] from numerical simulation of coarse-grained DNA, represented as sticky-end cylinders that can aggregate end-to-end. They find that a decrease in effective volume of the DNA fragments resulting from addition of salt leads to an increase in the critical concentration for ordering.

The above results on systems of DNA columns along with the results from PMF calculation demonstrate end-to-end stacking as a feasible mechanism for driving aggregates of very short blunt-end as well as shifted-end DNA fragments into nematic and other ordered phases like the columnar phase at high enough DNA concentration.

Structure of DNA columns.– To measure the relative orientation of the two DNA fragments in the blunt-end DNA columns, we calculate the azimuthal angle (φ), defined as the angle between the projections of the vectors joining O5′ and O3′ atoms of the terminal base-pairs onto a plane perpendicular to the common axis of the two stacked DNA fragments (Figure S8) [33]. We observe a marked difference between the φ distribution of the systems with the two initial configurations, FH and SH. The distributions are shown in Figures 4A-B for two different volume fractions. The distribution for the system with the initial SH configuration has two peaks, at around -25° and 135° whereas the one with initial FH configuration has a single peak at 135°. The initial and the final configurations for the two blunt-end DNA systems are shown in Figure S9A-B [33]. For SH initial configuration, the system seems to have two choices. This difference can be related to the shape of the energy profile of inter-DNA interaction as a function of φ. In case of FH, the system is probably close to a minimum in the free energy profile, whereas for SH the system is near a transition state, from where it can either fall to a given minimum or jump across the transition state towards a second minimum due to thermal fluctuations. The initial relative conformation between the DNA fragments in the FH configuration keeps φ close to 135°. Both -25° and 135° are closed configurations in terms of the exposure of terminal base pairs to water. In the -25° conformation the terminal GC base pairs show GC/GC stacking whereas the stacking is GC/CG for the 135° conformation (Figure S9) [33]. In the former, the 5′ ends of the DNA fragments

are in contact. Maffeo et. al. [44] in their study using atomistic simulation, also found two preferential values for the azimuthal angle. De Michele et al. [57] find the peak for end-to-end distance distribution at around 3.7 Å, while, Maffeo et al. [44] report peak at around 5 Å. The difference is attributed to the higher salt concentration of the system studied by De Michele et al. In the present study we obtain the peak at 3.7 Å eventhough the salt concentration is set to zero. While the nematic order parameter was affected by the addition of salt, the inter-DNA distance in a column showed no change at all and still peaked at 3.7 Å (Figure S9) [33].

III. CONCLUSIONS

In summary, we demonstrate that very short DNA fragments, as small as 4-bp long can stack strongly on top of each other and form persistent columns which can show nematic ordering over a large range of temperature. Prior to this study there were experimental and theoretical investigations on the behaviour of 6- to 20-bp long DNA fragments and the LC phases exhibited by them. We have shown that the formation of LC phases occurs for even smaller DNA fragments. As is well known that the formation of robust LC phase for rod shaped molecules also depends on the mechanical nature, like the persistence length, of the rods, in addition to their chemical nature. Such properties are expected to be different for columns formed by DNA fragments of different lengths. It is interesting to see that very small DNA fragments can give rise to columns sufficiently rigid to give rise to LC phase. Very recently, Fraccia et al. [7] have demonstrated LC phase for such short DNA fragments which our study compliments. The repulsive side-by-side interaction of blunt-end DNA is mostly governed by electrostatic interactions. The strength of end-to-end attraction is shown to be different for different relative azimuthal arrangements of the stacked blunt dsDNA fragments, demonstrating the hydrophobic nature of their end-to-end interaction. A transition from a strongly ordered nematic phase to a weakly ordered phase for a system of dsDNA columns takes place with a decrease in DNA volume fraction. The presence of a weakly ordered nematic phase rather than an isotropic phase at low volume fraction could be related to finite size effect. The relative azimuthal orientation of consecutive DNA fragments in a column show dependence on the initial configuration. The SH initial configuration gives rise to two different equilibrium relative configurations while FH gives rise to only one of them, which is very close to the FH configuration itself. This behavior may be related to the free-energy profile for end-to-end interaction between two dsDNA as a function of their relative azimuthal orientation. Although it may be noted that the more populated azimuthal orientations are all closed, in the sense that the interfacial base pairs of the two dsDNA are shielded from water. This behavior is in good agreement with the

behavior of the effective potential of interaction between a pair of dsDNA. Increasing temperature destabilizes the nematic ordering slightly, but the systems display strong ordering even at temperatures as high as 343 K. Adding monovalent salt also causes the equilibrium value of nematic parameter to decrease. The effect may be due to the screening of electrostatic repulsion between DNA fragments leading to an effectively less crowded environment resulting from a reduction in the effective excluded volume of a DNA column. The distance between DNA fragments in a column seems to be independent of the salt concentration. Thus, our study, in addition to quantifying the dsDNA interaction for various configurations, highlights the structural aspects of the DNA columns in the nematic phase and brings to light the dependence of ordering on various environmental factors, thus, providing inputs on the different behaviors expected in systems involving DNA self-assembly.

[1] A K Nayak, U Subudhi, RSC Adv. 4(97), 54506-11 (2014).

[2] P Chidchob, T G W Edwardson, C J Serpell, H F Sleiman, J. Am. Chem. Soc. 138(13), 4416-25 (2016).

[3] M Nakata, G Zanchetta, B D Chapman, C D Jones, J O Cross, R Pindak, P Bellini, N A Clark, Science 318, 1276-1279 (2007).

[4] J Lydon, Liq. Cryst. 38(11-12), 1663-81 (2011).

[5] T Bellini, G Zanchetta, T P Fraccia, R Cerbino, E Tsai, G P Smith, M J Moran, D M Walba, N A Clark, Proc Natl Acad Sci USA 109, 1110-1115 (2012).

[6] T P Fraccia, G P Smith, G Zanchetta, E Paraboschi, Y Yi, D M Walba, G Dieci, N A Clark, T Bellini, Nat Commun, 6, 6424-30 (2015).

[7] T P Fraccia, G P Smith, L Bethge, G Zanchetta, G Nava, S Klussmann, N A Clar, T Bellini, ACS Nano 10(9), 8508-16 (2016).

[8] T P Fraccia, G Zanchetta, V Rimoldi, N A Clark, T Bellini, Orig Life Evol Biosph 45(1-2), 51-68 (2015).

[9] G Zanchetta, M Nakata, M Buscaglia, T Bellini, N A Clark, Proc Natl Acad Sci USA 105, 1111-1117 (2008).

[10] G Zanchetta, F Giavazzi, M Nakata, M Buscaglia, R Cerbino, N A Clark, T Bellini, Proc Natl Acad Sci USA 107, 17497-17502 (2010).

[11] T E Strzelecka, M W Davidson, R L Rill, Nature 331, 457-460 (1988).

[12] R L Rill, Proc Natl Acad Sci USA 83(2), 342-346 (1986).

[13] T E Strzelecka, R L Rill, Biopolymers 30, 57-71 (1990).

[14] K Merchant, R L Rill, Biophys J 73, 3154-3163 (1997).

[15] K Kassapidou, W Jesse, J A P P van Dijk, J R C van der Maarel, Biopolymers 46(1), 31-37 (1998).

[16] J Olesiak-Banska, H Mojzisova, D Chauvat, M Zielinski, K Matczyszyn, P Tauc, J Zyss, Biopolymers 95(6), 365-375 (2011).

[17] G Zanchetta, T Bellini, M Nakata, N A Clark, J Am Chem Soc 130, 12864-12865 (2008).

[18] L Onsager, Annals of the New York Academy of Sciences 51, 627-659 (1949).

[19] P Bolhuis, D Frenkel J Chem Phys 106(2), 666-687 (1997).

[20] K T Nguyen, F Sciortino, C De Michele, Langmuir 30(16), 4814-4819 (2014).

[21] R Hentschke, J Herzfeld, Phys Rev A 44(2), 1148-1155 (1991).

[22] T Kuriabova, M D Betterton, M A Glaser, J Mater Chem 20, 10366-10383 (2010).

[23] K Shundyak, R van Roij, P van der Schoot, Phys Rev E 74, 021710 (2006).

[24] K R Purdy, S Varga, A Galindo, G Jackson, S Fraden, Phys Rev E 94, 057801 (2005).

[25] M Dennison, M Dijkstra, R van Roij, Phys Rev Lett 106, 208302 (2011).

[26] K T Nguyen, A Battisti, D Ancora, F Sciortino, C De Michele, Soft Matter 11(15), 2934-2944 (2015).

[27] H B Kolli, E Frezza, G Cinacchi, A Ferrarini, A Giacometti, T S Hudson, C De Michele, F Sciortino, Soft Matter 10(41), 8171-8187 (2014).

[28] Y M Yevdokimov, V I Salyanov, S G Skuridin, CRC Press, Boca Raton (2012).

[29] S Yasar, R Podgornik, V A Parsegian, Biophys J 108(2), 396a (2015).

[30] S Yasar, R Podgornik, V A Parsegian, Biophys J 106(2), 277a (2014).

[31] Y M Yevdokimov, S G Skuridin, V I Salyanov, E I Kats, Biophysics 61, 351 (2016).

[32] A A Kornyshev, D J Lee, S Leikin, A Wynveen, Rev Mod Phys 79, 943 (2007).

[33] See Supplemental Material at [URL] for the details of the restraints employed in the PMF calculation, structures of the DNA fragments used in this work, results of unrestrained simulations, temperature dependence of PMF for shifted-end DNA, side-by-side PMF for free-to-topple blunt DNA, arrangement of DNA columns, time evolution of nematic order parameter for the system of DNA columns at various volume fractions, definition of azimuthal angle and molecular details of the structure of DNA columns.

[34] P Mark, L J Nilsson, J Phys Chem A 105(43), 9954-9960 (2001).

[35] D A Case, T A Darden, T E Cheatham III, C L Simmerling, J Wang, R E Duke, R Luo, R C Walker, W Zhang, K M Merz et al., AMBER 12, University of California, San Francisco (2012).

[36] A Prez, I Marchán, D Svozil, J Sponer, T E Cheatham III, C A Laughton, M Orozco, Biophys J 92(11), 3817-3829 (2007).

[37] I S Joung, T E Cheatham III, J Phys Chem B 112(30), 9020-9041 (2008).

[38] J -P Ryckaert, G Ciccotti, H J C Berendsen, J Comput Phys 23, 327-341 (1977).

[39] H J C Berendsen, J P M Postma, W F van Gunsteren, A DiNola, J R Haak, J Chem Phys 81, 3684-3690 (1984).

[40] J-P Ryckaert, G Ciccotti, H J C Berendsen, J Comput Phys 23(3), 327-341 (1977).

[41] W Humphrey, A Dalke, K Schulten, J Mol Graphics 14(1), 33-38 (1996).

[42] G M Torrie, J P Valleau, J Comput Phys 23, 187-199 (1977).

[43] S Kumar, J M Rosenberg, D Bouzida, R H Swendsen, P A Kollman , J Comput Chem 13, 1011-1021 (1992).

[44] C Maffeo, B Luan, A Aksimentiev, Nucleic Acids Res 40(9), 3812-21 (2012).

[45] J SantaLucia Jr, D Hicks, Annu Rev Biophys Biomol Struct 33, 41540 (2004).

[46] P Yakovchuk, E Protozanova, M D Frank-Kamenetskii, Nucleic Acids Res 34(2), 564-74 (2006).

[47] T Bellini, R Cerbino, G Zanchetta, Top. Curr. Chem. 318, 225280 (2012).

[48] C Maffeo, J Yoo, J Comer, D B Wells, B Luan, A Aksimentiev, J Phys Cond Matt 26, 413101 (2014).

[49] A A Chen and A E Garcia, Proc Natl Acad Sci USA 110(42), 1682025 (2013).

[50] C Maffeo, R Schopflin, H Brutzer, R Stehr, A Aksimentiev, G Wedemann, R Seidel, Phys Rev Lett 105, 158101 (2010).

[51] B Luan, A Aksimentiev, J Am Chem Soc 130(47), 15754-5 (2008).

[52] A Savelyev, G A Papoian, J Am Chem Soc 129(19), 6060-1 (2007).

[53] M P Allen, G T Evans, D Frenkel, B M Mulder, Adv Chem Phys 86, 131-2 (1993).

[54] C B Stanley, H Hong, H H Strey, Biophys J 89(4), 255257 (2005).

[55] Potemkin II, N N Oskolkov, A R Khokhlov, P Reineker, Phys Rev E Stat Nonlin Soft Matter Phys, 72(2pt1), 021804 (2005).

[56] C De Michele, T Bellini, F Sciortino, Macromolecules 45(2), 1090-106 (2012).

[57] C De Michele, L Rovigatti, T Bellini, F Sciortino, Soft Matter 8(32), 8388-8398 (2012).